Lagrangian Study of Tropical Instability Vortices in the Atlantic

PIERRE DUTRIEUX

Department of Oceanography, University of Hawaii at Manoa, Honolulu, Hawaii

CHRISTOPHE E. MENKES AND JEROME VIALARD

LOCEAN, Université Pierre et Marie Curie, Paris, France

PIERRE FLAMENT

Department of Oceanography, University of Hawaii at Manoa, Honolulu, Hawaii

BRUNO BLANKE

LPO, Université de Bretagne Occidentale, Brest, France

(Manuscript received 12 January 2007, in final form 5 June 2007)

ABSTRACT

Tropical instability waves and tropical instability vortices (TIVs) exert major controls on ocean dynamics, thermodynamics, and biology on intraseasonal to seasonal time scales. To understand the fundamental mechanisms at play, a Lagrangian analysis of the 3D circulation of westward-propagating TIVs was performed in a high-resolution Atlantic Ocean simulation. The model reproduces the main temperature and velocity features of the tropical Atlantic mean state and the TIVs. Lagrangian diagnostics were used to track the water masses transported in vortices and exchanged with surrounding waters. The 3D circulation within vortices is consistent with previous observations and dominated by anticyclonic rotation with downwelling and upwelling near the leading and trailing edges of the vortex, respectively. This convergent flow creates sharp gradients at the TIV southwestern edge, where vertical mixing is most efficient. While TIVs remain highly dynamically coherent throughout their lifetime, significant exchanges occur with their surroundings, with 50% of their water being renewed over one rotation cycle. A detailed investigation of the eddies' sources and sinks reveals that they mostly transport southern water zonally, while northern waters are mostly passing through or fluxed southward in their lee. A notable source of entrained water is the Equatorial Undercurrent.

1. Introduction

In late boreal spring and summer in the tropical Atlantic and Pacific Oceans, the equatorial upwelling front exhibits north–south undulations on a scale of 1000 km (Legeckis 1977; Chavez et al. 1999) that shape the sea surface temperature and surface chlorophyll tracer fields in a series of troughs and crests. These patterns have been referred to as tropical instability waves (TIWs). They have periods of 25–35 days and have been shown to translate westward at speeds of 30–50 cm s^{-1} (Johnson 1996; Flament et al. 1996; Weidman et al. 1999; Kennan and Flament 2000; Chelton et al. 2000; Menkes et al. 2002).

There is no consensus on the mechanisms causing these instabilities; barotropic instability in the region between the South Equatorial Current (SEC) and the North Equatorial Countercurrent (NECC), baroclinic and barotropic instability between the Equatorial Undercurrent (EUC) and the SEC, and other processes, such as Kelvin–Helmholtz or frontal instabilities, have all been invoked (Philander 1976, 1978; Cox 1980; Luther and Johnson 1990; McCreary and Yu 1992; Yu et al. 1995; Qiao and Weisberg 1998; Donohue and Wimbush 1998; Masina et al. 1999; Kennan and Flament 2000; Johnson and Proehl 2004). A bifurcation analysis on a simplified linear model for the tropical

Corresponding author address: Pierre Dutrieux, Department of Oceanography, 1000 Pope Road, Honolulu, HI 96822.
E-mail: dutrieux@hawaii.edu

DOI: 10.1175/2007JPO3763.1

Pacific shows TIWs emerging from resonance between two equatorial Rossby waves (Lyman et al. 2005).

More recently, two different periods of unstable waves—a 17-day Yanai wave within 2° of the equator and a 33-day Rossby wave around 5°N—have been reported in the tropical Pacific (Lyman et al. 2007). These two waves are likely to interact north of the equator, where fully developed TIWs are nonlinear (Kennan and Flament 2000) and are associated with anticyclonic eddies, or tropical instability vortices (TIVs; in order to emphasize their near-closed circulation), which may be about 500 km in diameter, are responsible for the undulating shape of the equatorial front and are clearly revealed by surface drifter trajectories (Hansen and Paul 1984; Flament et al. 1996; Kennan and Flament 2000; Menkes et al. 2002; Foltz et al. 2004).

Both Atlantic and Pacific vortices have a complex three-dimensional (3D) circulation from the surface down to the thermocline. At the leading edge of the vortex, the flow decelerates, resulting in convergence, downwelling, and frontogenesis (Yoder et al. 1994; Flament et al. 1996; Archer et al. 1997; Menkes et al. 2002). As the flow recirculates anticyclonically, upwelling occurs from the trailing edge to the center of the vortex. TIVs thus redistribute mass, heat, salt, and tracers, and influence the equatorial ecosystem in complex ways (Strutton et al. 2001; Menkes et al. 2002). For example, while individual vortices are seen to strongly shape the ecosystem and increase chlorophyll concentration in their leading edge, the net effect of TIVs on biology at seasonal time scales is to decrease primary production in the equatorial Pacific (Gorgues et al. 2005). Similarly, TIVs are primarily visible as a northward intrusion of cold upwelling water, but their resulting effect on the heat budget is a warming of the equatorial SSTs, which is of a similar magnitude to the seasonal heat forcing effect (Hansen and Paul 1984; Flament et al. 1996; Baturin and Niiler 1997; Swenson and Hansen 1999; Kennan and Flament 2000; Jochum and Murtugudde 2006; Menkes et al. 2006; Peter et al. 2006). Simulations in the Pacific and Atlantic Oceans suggest that eddy-induced horizontal advection is a major heating term for sea surface temperature (SST), and vertical diffusion at the base of the mixed layer is a cooling term (Jochum and Murtugudde 2006; Menkes et al. 2006; Peter et al. 2006). In a TIV, the mixed layer and the top of the thermocline are largely decoupled. As TIV dynamics extend down to the thermocline (Kennan and Flament 2000; Menkes et al. 2002), the processes by which they redistribute mass, heat, salt, and biological fluxes are different within the mixed layer and below it. For instance, vertical diffusion cools the mixed layer while it warms the water just below. Similarly, vertical advection of heat is negligible at the mixed layer base, but becomes significant below (Menkes et al. 2006). Based on mixed layer potential vorticity budgets in a simulation of the Atlantic, Foltz et al. (2004) estimated an annual northward cross-equatorial transport of up to 1.2 Sv (1 Sv $\equiv 10^6$ m^3 s^{-1}) resulting from TIVs' acquisition of Southern Hemisphere water along their paths. Because the vortex dynamics of Foltz et al. (2004) are not confined to the mixed layer, their flux estimates may be biased. Finally, an SST study by Jochum and Murtugudde (2006) proposed that TIWs redistribute surface heat by advecting water back and forth meridionally across an equatorial region of large vertical entrainment. The authors point out the need for a Lagrangian exploration to understand the exact pathways leading to heat redistribution. This is even truer if one is interested in extending TIV-induced SST changes to the full impact of TIVs, down to the top of the thermocline. These considerations underline the importance of precisely understanding TIVs' 3D circulation, their contribution to the water mass and their exchanges with their surroundings. Toward this end, a Lagrangian trajectory computation will be performed in a high-resolution simulation on the tropical Atlantic region. The following questions will be addressed: are the flow patterns associated with TIVs coherent during their lifetime? How is water redistributed in a TIV? Are TIVs closed structures, or do they exchange mass and tracers with adjacent waters (and if so, how)? A detailed description of the TIV flow and exchanges is a necessary step toward understanding impacts of TIVs at broader scales and on the biogeochemical system.

Section 2 is devoted to data and model presentation. In section 3, the model solution is evaluated with respect to observations. Section 4 presents the Lagrangian trajectory experiments. Section 5 describes the TIV-induced circulation and their general characteristics in the model. In section 6, advective transfers from vortices to adjacent waters are quantified and characterized. The results are summarized and discussed in section 7.

2. Means of study

a. Observations

In situ observations from the Production Induite en Zone de Convergence par les Ondes Longues (PICOLO) sea experiment (June 1997) are used to explore dynamical conditions of the tropical Atlantic region (0°–8°N, 30°–20°W) in the presence of TIVs (Menkes et al. 2002). Horizontal ocean currents were measured using a shipboard 150-kHz acoustic Doppler current profiler (ADCP) and 10 surface drifting buoys

(Niiler et al. 1987). Following Menkes et al. (2002), drifter velocities are regridded in a translating frame of reference moving westward at 35 cm s^{-1}. Vertical velocities are derived from depth integration of horizontal currents' divergence assuming a rigid lid. Every 20 n mi temperature and salinity profiles were obtained to 250-m depth.

Weekly averaged SST obtained for summer of 1997 from Pathfinder Advanced Very High Resolution Radiometer (AVHRR) data (online at http://podaac.jpl.nasa.gov/sst/sst_data.html) is used on a 9-km grid.

b. The CLIPPER model

The Atlantic model CLIPPER, version ATL6-V6 (CLIPPER Project Team 2000) is based on the code developed by Madec et al. (1998) and solves the primitive equations with a finite difference scheme on an Arakawa (1972) C grid. It has a horizontal Mercator grid with 1/6° resolution and 42 vertical levels, with 20 levels in the upper 200 m. It is initialized by the Reynaud et al. (1998) temperature and salinity climatology. All forcing fields (except wind stress) are taken initially from the daily climatology of the 15-yr European Centre for Medium-Range Weather Forecasts (ECMWF) Re-Analysis (ERA-15; Gibson et al. 1997) reanalyzed flux, which covers 1979–1993, and then from the actual ECMWF analysis for 1994–2000. Daily wind stress is linearly interpolated from the weekly gridded product based on European Remote Sensing Satellites observations (information online at http://www.ifremer.fr/cersat). Vertical diffusion of momentum is solved by a 1.5 turbulent kinetic energy closure scheme (Blanke and Delecluse 1993), with background value of 10^{-4} m^2 s^{-1}. Horizontal momentum diffusion is simulated by a bi-Laplacian with a coefficient of 5.5×10^{10} m^4 s^{-1} at the equator, and varying as the third power of the grid spacing away from the equator. To parameterize unresolved inertial instabilities at the equator, a Laplacian diffusion of momentum (with a constant coefficient of 1000 m^2 s^{-1}) was added at the surface within 1° of the equator, decaying exponentially poleward (Richards and Edwards 2003). Mixing of the tracers is isopycnal, following Lengaigne et al. (2003).

Focusing on the PICOLO experiment time frame, we analyze the year 1997 of the interannual simulation. Daily means are used here for May, June, and July 1997, when TIVs are most active.

3. Model evaluation

a. Low-frequency variability

A parallel study (Peter et al. 2006) compares the simulation with observations at seasonal to interannual time scales. There is, in general, good agreement. The SEC and the NECC are well localized, with their dynamical boundary at about 3.5°N, the typical latitude of origin of TIVs. Realistic seasonal cycles of current are reproduced. In the vertical, the mean thermocline depth and its interannual and seasonal variabilities are well captured. However, the thermocline is too diffuse at the equator, and comparison to observed SST shows a cold bias along the equator (1°C) that is more pronounced to the west, which is a common shortcoming of equatorial models.

b. High-frequency variability

Despite model biases, the simulation of TIVs is encouraging. Cusp-like undulations of the surface fronts in temperature have already been observed on Pathfinder AVHRR SST during the boreal summer of 1997 (Menkes et al. 2002). Figure 1 compares snapshots of simulated SST with the satellite observations. The TIVs appear about 1 week later in the simulation. Meridional undulations of the north equatorial front (NEF) delimiting the cold tongue are confined between 1° and 5°N. Interestingly, similar patterns develop south of the equator with similar wavelengths and slight spatial lag. This was also noted in the Pacific by Chelton et al. (2000). The model reproduces the spatial expansion and temperature gradient patterns of the TIVs quite well east of 30°W. In the west, however, the modeled SST is too cold. Because TIWs are sensitive to meridional temperature gradients, the discussion will be restricted to the central and eastern parts of the tropical Atlantic. A zoom on one vortex (see box in Figs. 1a,b) is shown in Figs. 1c–j. Both the model and observations show vortices of about 500-km diameter, with radial speeds of about 1 m s^{-1}. Downwelling occurs in the coldest southeast portion of the vortex, while upwelling is found in warm SSTs from the eddies' western edge to their center (Figs. 1d,f). These patterns are also commonly found in the Pacific Ocean. Since the Tropical Instability Wave Experiment (TIWE) (Kennan and Flament 2000), TIVs are known to be nonlinear, with Rossby numbers on the order of unity. This is illustrated in Figs. 1h,j, displayed relative to the planetary vorticity ratio of −1 in our simulation and observations. They also are vorticity-dominated regions, surrounded at their edges by strain-dominated regions. This is illustrated in Figs. 1g,j, displaying the Okubo–Weiss parameter (Okubo 1970; Weiss 1981; Pasquero et al. 2001). In the vortex center, the Okubo–Weiss parameter is relatively negative, suggesting weak water dispersion. Along its edges, and especially in the west-southwest convergence zone, the Okubo–Weiss parameter is relatively positive, suggesting strong water dispersion. Al-

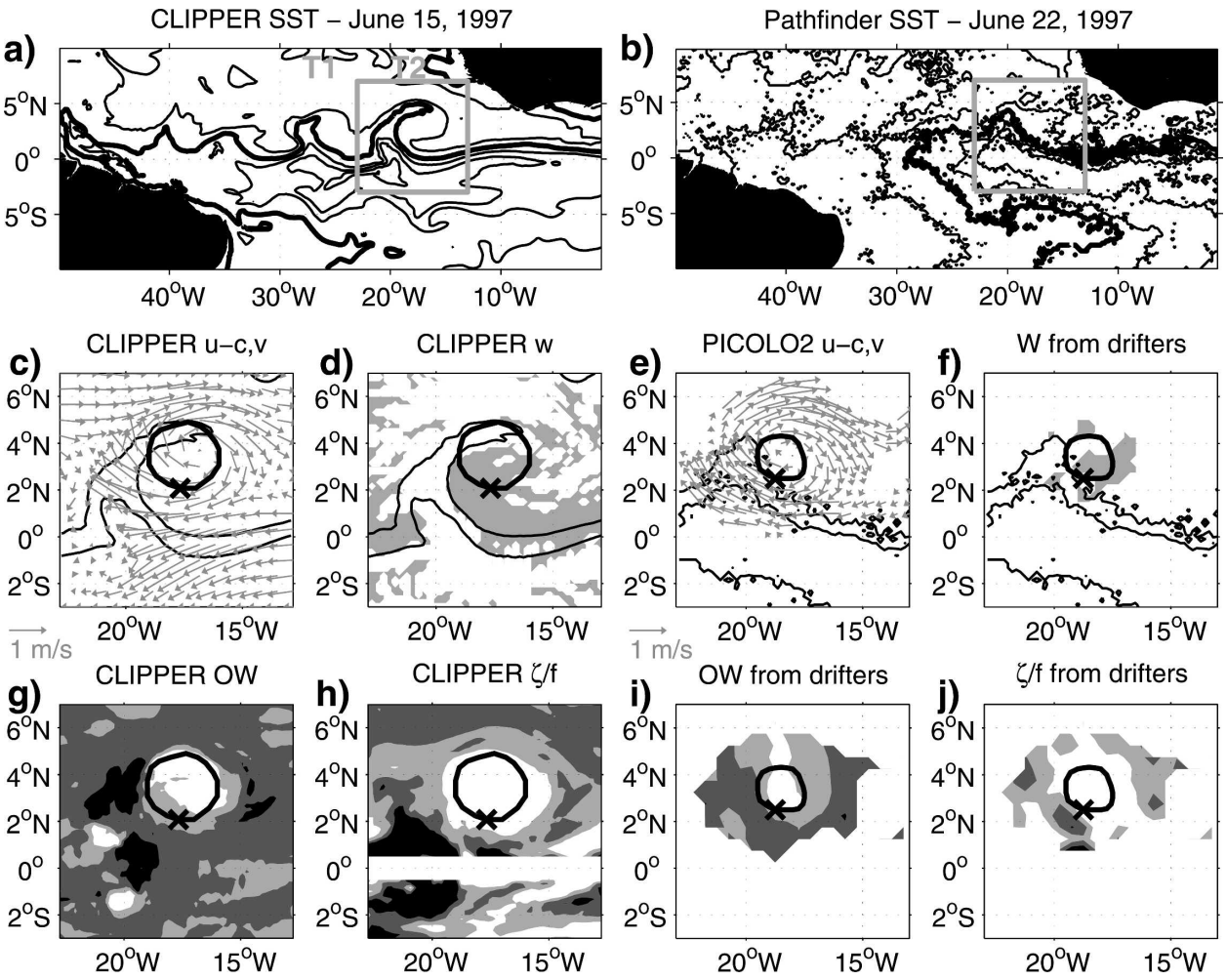

FIG. 1. (a) CLIPPER model SST averaged from 13 to 17 Jun 1997 at a 1°C contour interval, with the 25.5 contour in thick black; colder temperatures are found at the equator. (b) Pathfinder AVHRR SST on 22 Jun 1997, with the same contours as in (a). (c), (e) Zoom, respectively, on square regions indicated in (a) and (b), showing CLIPPER and Pathfinder 24° and 25.5°C SST contours (black thin solid line), CLIPPER and PICOLO drifter surface velocity vectors (gray arrows) in a frame of reference moving westward at 32 cm s^{-1}, and a closed streamline (thick solid black). The black star indicates the starting point of the vertical sections shown in Fig. 4. (d), (f) Respectively, positive vertical velocity in CLIPPER and PICOLO from drifter velocity in gray shading, with 24° and 25.5°C CLIPPER and Pathfinder SST contours. (g), (i) Respectively, Okubo–Weiss parameter in CLIPPER and PICOLO from drifter velocity in gray shading, with contours of -5×10^{-10}, 0, 5×10^{-10} s^{-2} from white to black. (h), (j) Respectively, the ratio of relative to planetary vorticity in CLIPPER and PICOLO from drifter velocity in gray shading, with contours of −0.5, 0, and 0.5 from white to black. Values of −1 are reached within the vortex.

though this parameter is not suitable for studying 3D time-evolving flows, it gives a qualitative snapshot view of the dispersion topology.

Figure 2 shows that periods (about 20 days) and wavelengths (1000 km) are well represented in the simulation. TIVs move westward at a speed of 30 cm s^{-1} in the Atlantic (Chelton et al. 2000; Menkes et al. 2002), with faster propagation speeds in the center of the basin.

In the remaining examination, for statistical representation, we will focus on the two most prominent propagating TIVs, respectively labeled T1 and T2 in Figs. 1 and 2. Both travel across the central Atlantic in the model and the observations.

Figure 3 compares vortex T2 with the PICOLO observations at 20°W. The simulated eddy here is centered slightly south of the observed one, which leads to a southward shift of all modeled characteristics. At the equator, the simulated EUC is slightly too energetic (1 m s^{-1}; that is, 10 cm s^{-1} more than observed). The anticyclone extends from the surface to the top of the thermocline, which is well fitted by the 21°C isotherm.

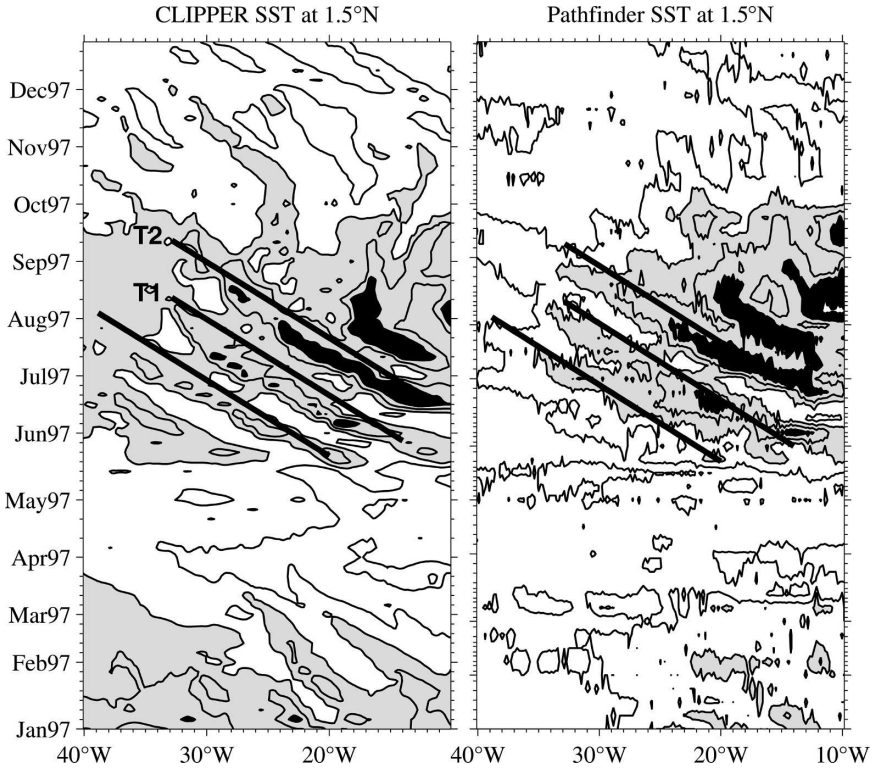

FIG. 2. Longitude–time diagram of SST for (left) CLIPPER and (right) Pathfinder at 1.5°N at 1°C contour intervals, with values lower than 24°C shaded in gray and those lower than 22°C shaded in black. Thick solid lines indicate 32 cm s^{-1} westward propagation speed. The two propagating structures T1 and T2 are labeled.

The SEC, which reaches speeds greater than 50 cm s^{-1} above 50-m depth at 2°N, is more surface intensified in the observations. At 5°N, the NECC flows eastward at about 80 cm s^{-1}. Similar to Pacific observations by Kennan and Flament (2000), these vertical sections reveal a meridional asymmetry in velocity, with the core of maximum speed being deeper in the north. The thermocline is deepening near the center of the eddy, with a more diffuse NEF in the simulation. Fresher water is found above the thermocline north of the NEF, both in the observations and in the model, near 3°–4°N. Below, at the thermocline depth, relatively saline waters connect from south to north, suggesting the export of high-salinity equatorial water by the vortex at its base (another feature reported by Kennan and Flament 2000).

Overall, zonal and meridional speeds are reasonably simulated. To better understand the circulation, we choose to display sections of velocity and temperature along closed streamlines (displayed in Fig. 1) of the surface current in TIV T2 (Fig. 4). The streamlines were chosen such that the distance to the cold front is approximately the same in both the simulation and the observations, which have a better sampling near the center of the eddy. Beginning south-southwest (as indicated by the star in Fig. 1), colder and saltier (not shown) water is upwelled and advected to the northwest, away from the equator. At the NEF, it encounters downwelling (see also Figs. 1e,f) and subducts under warmer and fresher (not shown) north tropical surface water. Following the streamline, water upwells to connect to the equatorial region. These vertical displacements feature, off the equator, vertical speeds up to ± 15 m day^{-1}, that is, an order of magnitude greater than the velocities typical of equatorial upwelling (Weingartner and Weisberg 1991).

Both datasets remarkably agree along the streamlines. More generally, the CLIPPER simulation exhibits good skill in reproducing the main observed features during TIV activity periods. Therefore, we turn confidently to the model analysis to investigate physical processes at work during the summer of 1997.

4. Method and Lagrangian experiments

Because the TIV involves 3D advective processes, a Lagrangian point of view is natural. We will use Lagrangian tracking of fictive water particles to determine the circulation within the TIVs and their exchanges with surrounding waters.

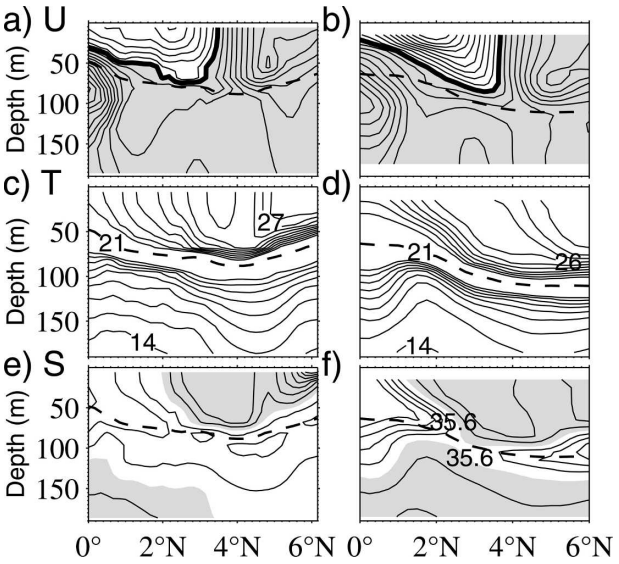

FIG. 3. (left) Meridional sections down to 200-m depth of 5-day-averaged model fields on 30 May 1997 at 20°W, and (right) equivalent section for the PICOLO experiment, at 20°W. (a), (b) Zonal velocity in the translating frame of reference, with a 10 cm s^{-1} contour interval. Shading indicates positive values. Zero velocity contour in thick black. (c), (d) Temperature with a 0.5°C contour interval, with a gap between 18° and 23°C. (e), (f) Salinity with 0.1 contour interval, with a gap between 35.5 and 35.7. Shading indicates a salinity less than 35.6. In all plots, the dashed line indicates the 21°C isotherm, a proxy for the thermocline depth.

a. A TIV structure definition

A definition of the evolving TIV volume is first needed. In a two-dimensional flow, the Okubo–Weiss parameter has been successfully used to distinguish vorticity-dominated regions from strain-dominated regions (Bracco et al. 2000; Pasquero et al. 2001; Isern-Fontanet et al. 2004). However, our concern is 3D. A radially uniform and monotonous variable enclosing vortices is more practical. Based on the TIWE and PICOLO experiments (Kennan and Flament 2000; Menkes et al. 2002), we chose to define the vortex as horizontally confined by the surface streamfunction above a threshold of 2.5×10^5 s^{-1}. In the vertical, TIV motions are mostly homogeneous down to the top of the thermocline. Thus, the surface structure is directly extended to the top of the thermocline, which is well fitted by the 21°C isotherm (Figs. 3 and 4). An example of the resulting vortex volume is depicted in Fig. 5c.

There is no unique way to define a vortex entity. We are aware of the arbitrary nature of our definition in general, and of the threshold value in particular. However, this method allows us to describe closed volumes and their exchanges with their surroundings, which is our main goal. This will be discussed further in the conclusions.

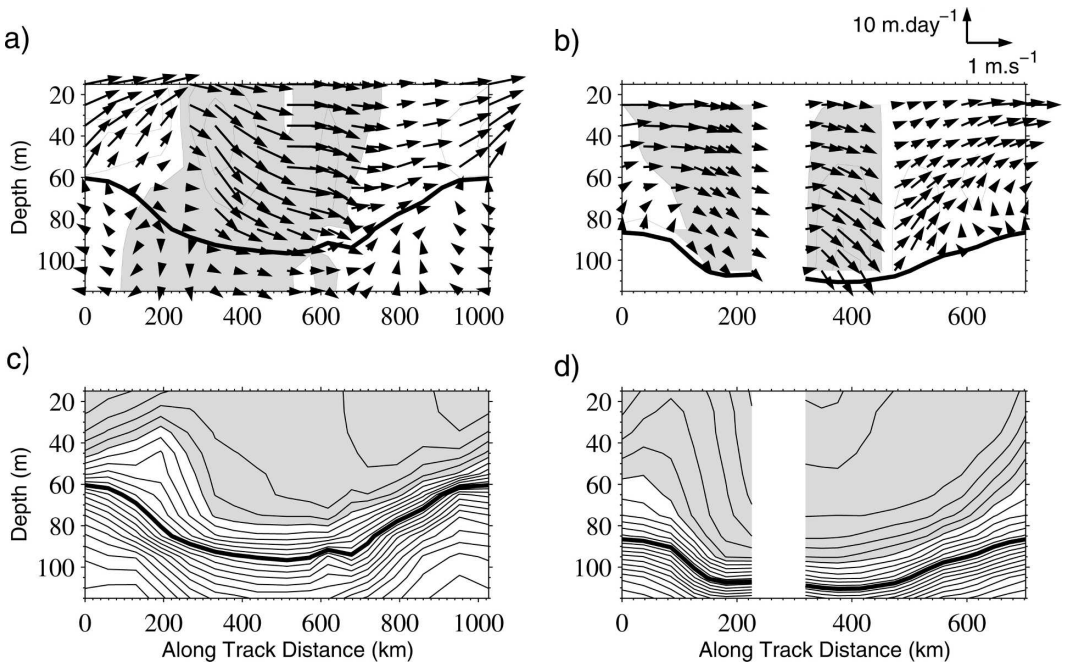

FIG. 4. Vertical sections along the closed streamlines shown in Fig. 1, starting from the star drawn in Fig. 1 for the (left) CLIPPER model and (right) PICOLO experiment. (a), (b) Vertical velocity with a 5 m day^{-1} contour interval. Downward velocities are shaded. Vectors represent velocity in the vortex frame of reference translating westward at 32 cm s^{-1}. (c), (d) Temperature with a 0.5°C contour interval. Temperatures colder than 24°C are shaded. In all plots, the thick solid line indicates the 21°C isotherm, a proxy for the thermocline depth.

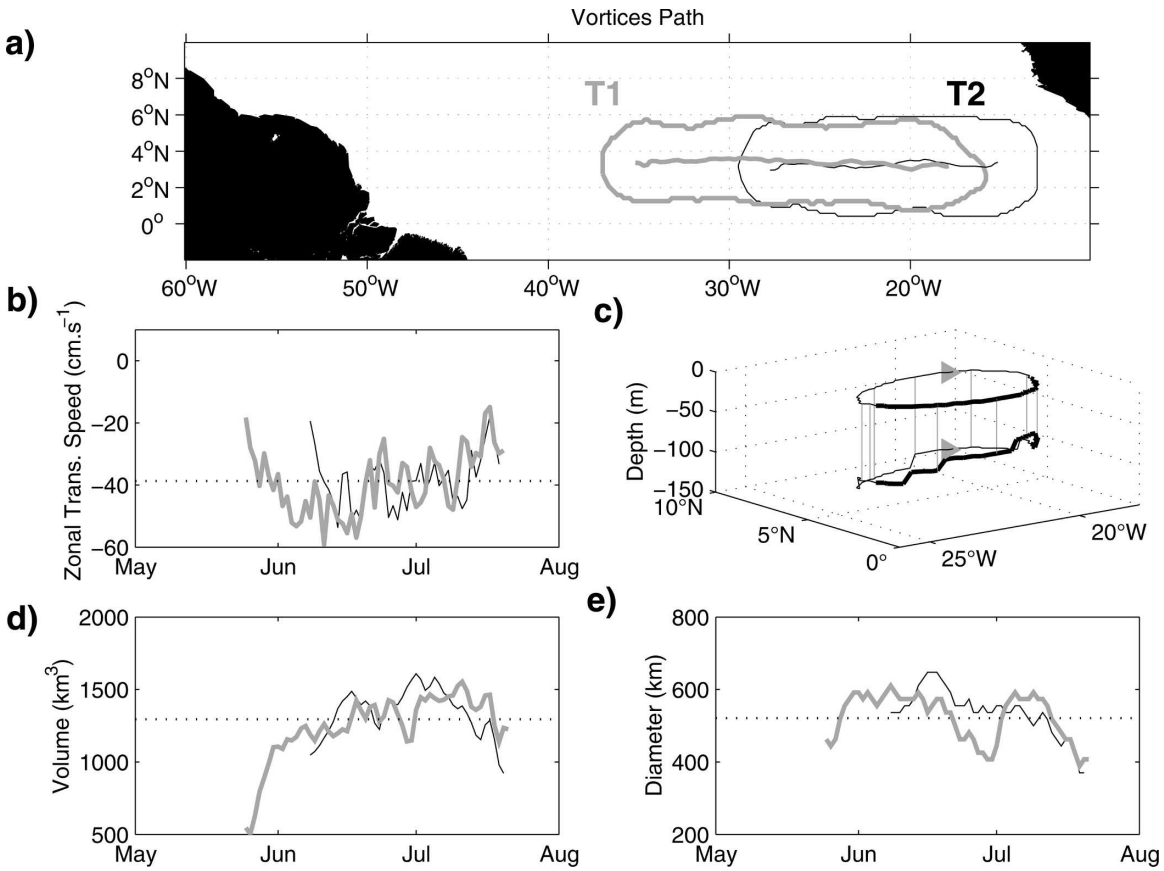

FIG. 5. (a) Envelopes of vortices T1 (gray thick solid line) and T2 (black thin solid line) and trajectories of their centers across central tropical Atlantic. (b) Zonal propagation speed of the vortices' centers. (c) Structure of T2 as defined in section 4a for 24 Jun 1997. Time series of (d) vortex volumes and (e) vortex diameters. In (b), (d), and (e), the thick gray line and thin black line refer to T1 and T2, respectively.

b. Lagrangian experiments

To compute trajectories of fictive particles within the simulated 3D current field we use the ARIANE package (Blanke and Raynaud 1997). This tool allows offline forward and backward 3D tracking. If desired, fictive particles can be maintained at a constant depth. Using our vortex structure definition (section 4a), we follow T1 and T2 over 60 days in the daily averaged fields (Fig. 5). We are now able to determine whether particles enter, exit, or remain in an eddy for every model day. We aim at 1) describing the TIVs' 3D circulation, 2) exploring their time consistency and associated implications for enclosed tracers, and 3) characterizing and quantifying the TIVs' exchange with their surroundings. Toward these goals, we devised two main experiments.

The first experiment, labeled E1, consists of seeding each grid point at 18-m depth over a rectangular domain centered on vortex T2 on 8 July 1997, at the beginning of its course in the tropical Atlantic (Fig. 6a). The domain is 10° longitude and 8° latitude. ARIANE is then run forward for 55 days for two separate configurations: in configuration E1-2D, fictive particles are forced to remain at their initial depth, thus yielding 2D trajectories; in configuration E1-3D, on the contrary, particles are free to evolve vertically.

The second experiment, labeled E2, consists of two ensembles of 50 3D trajectory computation sets. It takes about 50 days for T1 or T2 to reach 30°W (Fig. 2). For each of these 50 consecutive days, and separately for T1 and T2, a water volume with a horizontal dimension identical to that of E1, but extending from 0- to 200-m depth, is seeded. Forward and backward analyses are then performed over 20 days (i.e., one TIV rotation cycle). This creates two ensembles (for T1 and T2) of fifty 20-day trajectory sets allowing ensemble averages with statistical significance. Each trajectory is analyzed separately to determine which particles stay in, leave, or enter an evolving vortex structure in 20 days. Particles that remain at least 20 days in a TIV are qualified as captive particles. Inversely, particles that

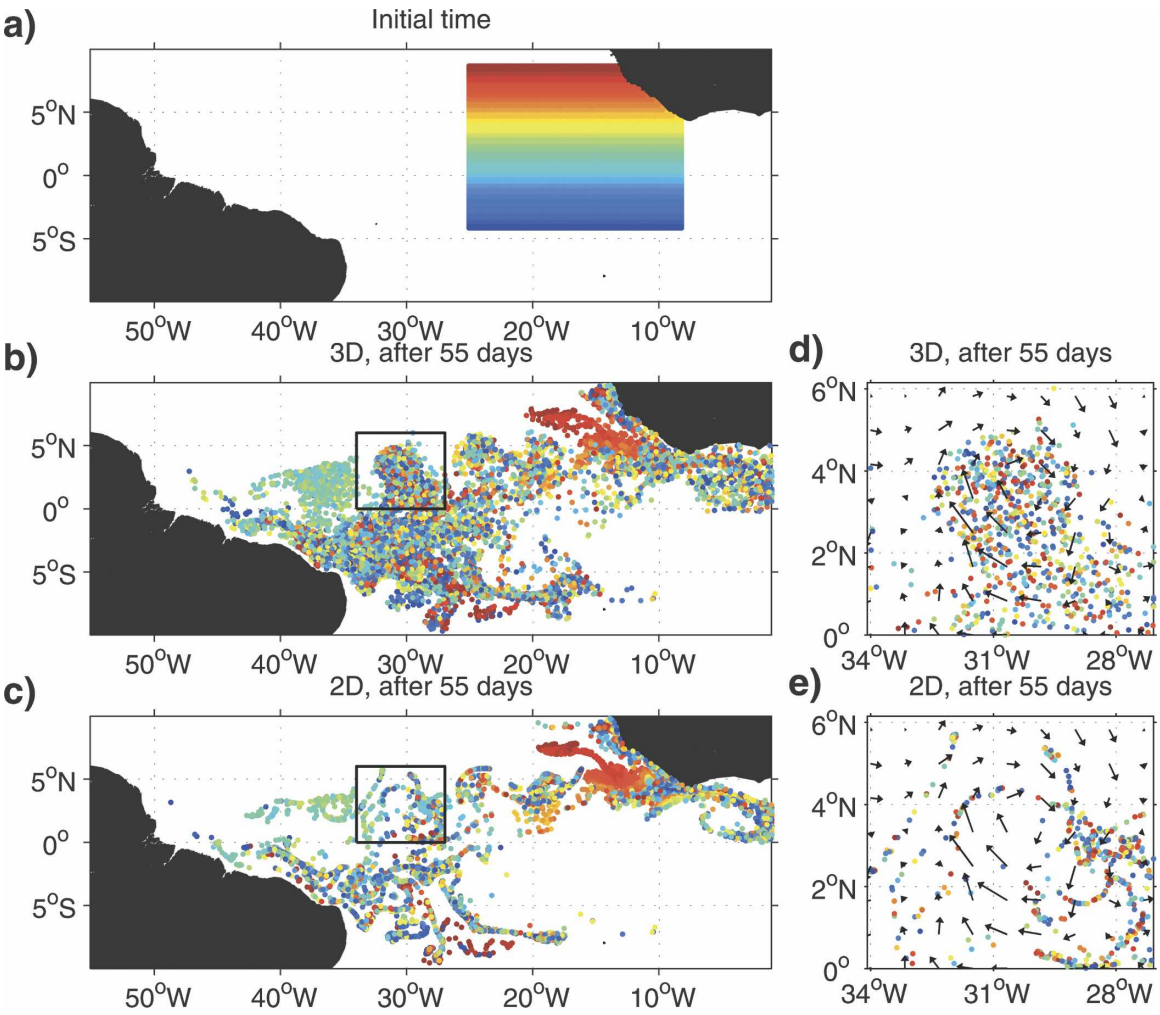

FIG. 6. (a) Initial positions of particles in experiment E1-2D and E1-3D, color-coded as a function of initial latitude. Position of the same particles 55 days later in (b) E1-3D and (c) E1-2D. Vortex T2 is initially centered at 18°W, and propagates as far as 30°W after 55 days [black box in (b) and (c)]. (d), (e) Zoom over the black boxes drawn in (b) and (c), respectively. Vectors show surface currents.

are in a TIV and are not in it the following day are qualified as leaving particles; particles that are not in a TIV and then are in it the following day are called entering particles. The computation of the ratio between the particle numbers crossing the 21°C isotherm (the base of our vortex definition) and the total number of particles in the vortex gives less than 0.2%. Our definition of the vortex base is thus adequate.

5. A coherent 3D circulation within TIVs

In their analysis, Flament et al. (1996), Kennan and Flament (2000), and Menkes et al. (2002) hypothesized that TIV flow characteristics remain similar over a 1–2-month time scale. Simulations recently corroborated this assumption in the Atlantic (Foltz et al. 2004) and Pacific (Menkes et al. 2006).

a. General characteristics

The CLIPPER simulation is consistent with this result in the Atlantic: our vortex structure definition (section 4a) allows a comprehensive description of TIV basic characteristics, represented in Fig. 5, for about 2 months. Both T1 and T2 move westward along 3.5°N, with remarkably steady diameters of around 500 km.

Their mean propagation speed is 38 cm s^{-1}, which is a value similar to another model result by Foltz et al. (2004) but slightly faster than observed speeds. In CLIPPER, T1 and T2 have two major evolution phases. At the beginning of their life cycle, their propagation speed increases from 20 to more than 40 cm s^{-1}, as their initial volume grows. Their speed then slowly decays, as their volume remains stationary (around 1300 km^3). Their path, followed for 55 days, encompasses the east

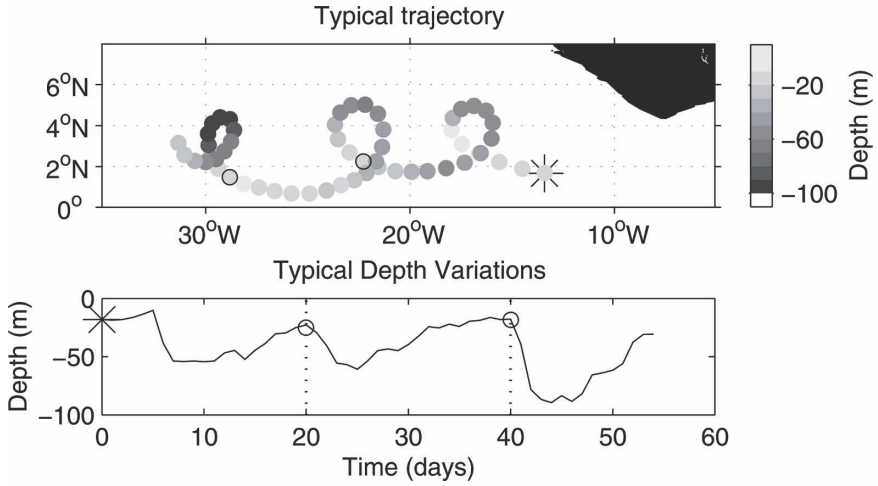

FIG. 7. (top) Typical track for a particle entrained in a TIV, with a daily sampling of positions and a color code related to the depth of the particle. The star symbol indicates the initial position and one black circle is drawn every 20 days, for time reference. (bottom) Time series for the depth of the same particle.

to central Atlantic, at 1°–6°N, 13°–37°W. Their vertical shape is characterized by the northward downward tilt of the thermocline at their base (Fig. 5c).

b. A 3D process

In the data analyses from Flament et al. (1996), Kennan and Flament (2000), and Menkes et al. (2002), it is hypothesized that surface drifters can track individual vortex circulation with some confidence over one period. Yet, we have seen that TIV circulation is 3D. Thus, we wish to assess the difference of circulation inferred from both surface and 3D floats (Fig. 6). The general characteristic of E1-3D to show a more homogeneously spread particle field than that of E1-2D is striking (note that all of Fig. 6 shows the same number of particles). When floats are constrained to remain at a constant depth (here, at 18 m), they tend to concentrate in downwelling regions. For instance, in the Northern Hemisphere, E1-2D particles tend to align along the convergence between the NECC and the SEC between 15° and 40°W. Describing surface circulation with 2D floats thus undersamples divergence areas (upwelling) such that the equatorial region is depleted (Fig. 6c). In contrast, 3D floats have homogeneously paved the basin (Fig. 6b). After 55 days, vortex T2 is centered around 30°W. In E1-3D, T2 contains both Northern and Southern Hemisphere water and is filled with particles, indicating strong meridional exchanges. In E1-2D, on the contrary, significantly fewer particles remain in the vortex. This is reminiscent of the general idea that TIV circulation is coherent in 3D, but becomes chaotic as one tries to describe it in a constrained 2D field, restraining the number of possible trajectories and congregating particles in manifolds (Haller 2000). These results show that the TIV circulation cannot be adequately described by surface floats followed for 55 days. Another notable feature here is the particle redistribution between the Northern and Southern Hemispheres in which TIVs play an active role, as will be seen in following sections.

Yet, our calculations show that the deviation of the E1-2D captive particle trajectories from E1-3D is becoming important only after one rotation period (not shown), that is, after about 20 days. This explains both the ability of previous studies to base their analyses on surface float trajectories showing cycloidal behavior for some 25 days (Kennan and Flament 2000; Menkes et al. 2002), and the scarcity of floats exhibiting the same behavior for longer time scales.

We now turn to the 3D description of TIV circulation. Data and the model alike suggest that a typical water mass entrained in a TIV is moved away from the equator, is downwelled near the leading edge of the vortex, circuits at depth, and returns to the equatorial surface layers as upwelling occurs. The trajectory of a particle from experiment E1-3D that remains in vortex T2 is plotted in Fig. 7. It indeed displays a cycloidal trajectory with a marked upwelling/downwelling feature. The particle loops almost 3 times in the vortex, in about 55 days, experiencing successively sharp downward and slower upward movements, with 50-m amplitudes, as it passes through the convergence and divergence regions. This pattern suggests that a typical time scale for the rotating period is about 20 days, a time that

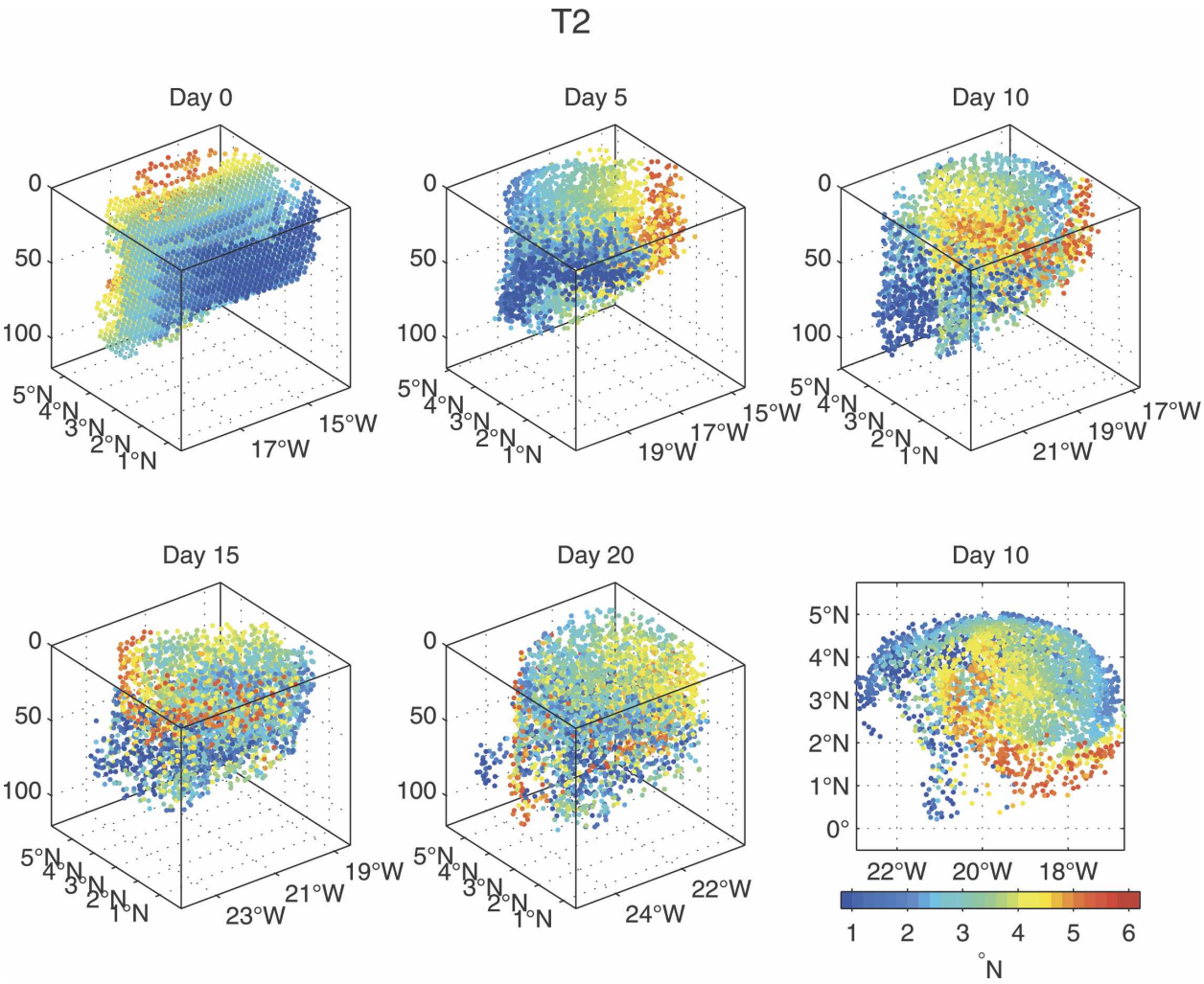

FIG. 8. Successive 3D positions of particles captured in T2 on 18 Jun 1997 that will be in it 20 days later. Particles are colored as a function of their initial latitude. (bottom right) Horizontal projection of the top right.

is consistent with observations in the Pacific and the Atlantic Oceans (Kennan and Flament 2000; Menkes et al. 2002).

Keeping in mind the individual trajectory, we show one sequence (representative of the 50 other possible choices) of those evolving particles enclosed in T2 during 20 days (Fig. 8). While rotating anticyclonically, particles from the north upwell and concentrate in the upper vortex layers (day 5), partly spiraling toward the vortex interior (day 10). The spiral effect is better depicted in the lower-right panel. In addition, one sees that these particles are dispersed as they rotate, indicating that the vortex is not in solid body rotation as previously hypothesized (Flament et al. 1996; Kennan and Flament 2000; Menkes et al. 2002). These particles continue their rotation at the surface with some spiraling from the center to the edges at the surface (day 15–20), and others located at the edges on day 10 and sinking at the front (days 15–20) (not shown). Similarly, particles initially located in the southern part of the vortex spiral down and disperse along the path in the vortex interior, leading, on day 10 (half-period), to a "yin–yang" pattern. The deepest among these particles on day 10 remain at depth while others upwell back to the surface layer (days 15–20). These complex redistributions are possible because the flow, while coherent, is not steady and is 3D. This allows for a complete 3D water mass redistribution within the vortex in one period (cf. days 0 and 20), with water from the NECC region being mixed with water from the upwelling region. Given that our surface forcing does not vary at such scales, tracing water mass characteristics for the moving particles (e.g., temperature, density, etc.) will give an estimate of mixing in the TIV.

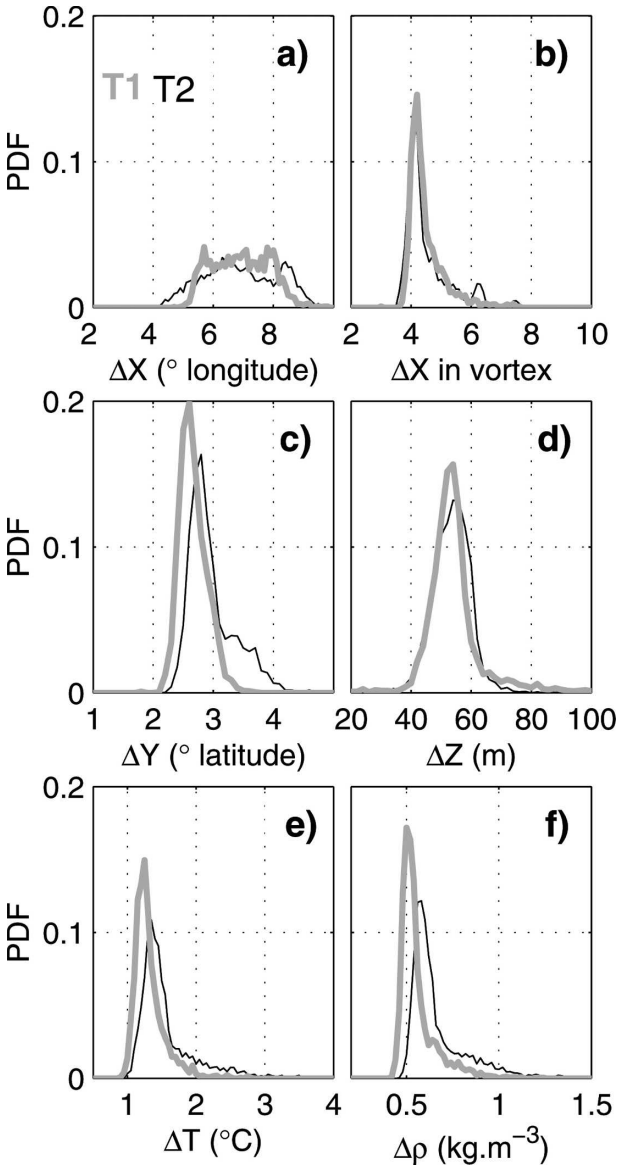

FIG. 9. Probability density function of maximum changes occurring to particles that remain in a TIV for at least 20 days: T1 (thick solid gray line) and T2 (thin solid black line). (a) Maximum zonal displacement (°), (b) maximum zonal displacement in the vortex frame of reference (°), (c) maximum meridional displacement (°), (d) maximum vertical displacement (m), (e) potential temperature change (°C), and (f) potential density change (kg m^{-3}).

c. Lagrangian variability within TIVs

The coherence of those characteristics is estimated statistically by computing the maximum displacement or maximum tracer change occurring within one cycle (20 days) for every water particle remaining in T1 and T2 for each of the 50 days of insemination (see the experiment E2 description). Figure 9 shows their ensemble-averaged distributions. Characteristics for T1 and T2 are quite similar and show the robustness of the results. The relative sharpness of these distributions is indicative of a high coherence in all captive particle circulations, typically described in Fig. 7. In a fixed reference frame, most particles entrained in a TIV travel 6°–8° zonally, more than the vortex mean diameter (500 km), which clearly shows that these vortices transport mass to the west. In a frame of reference moving with the vortex, particles experience maximum zonal excursions of 4° and meridional displacements between 2.5° and 3.5°. They experience 40–70-m depth variations. These displacements are consistent with the 3D description of the vortex circulation given in the previous section. It is worth noting that the limited zonal and meridional displacements compared with the vortex diameter (5°) confirms the spiraling movements seen on Fig. 8 and shows that modeled vortices are not in solid body rotation. Water masses in the vortex experience 1°–2°C and 0.5–1 kg m^{-3} changes in 20 days. This marks important diapycnal mixing inside a vortex structure.

Figure 10 gives insight on the processes leading to such mixing. In a frame of reference moving with the vortices, experiment E2 trajectories are analyzed to give the Lagrangian derivative of temperature, simply given by the day-to-day difference of temperature following the trajectory as a function of depth, the distance from the vortex center, and the polar angle from the east direction. For T1 and T2, respectively, we have ensembles of 50 realizations. We then apply the ensemble average. Averaging the Lagrangian derivative over the TIV depth yields an estimate of the heat stored therein. Because lateral diffusion can be neglected here (a small term in our simulation; Peter et al. 2006), the depth-averaged Lagrangian derivative is equal to the heat flux balance between the atmospheric flux and vertical diffusion heat flux at the TIV base, redistributed in the TIV by vertical diffusion. As before, we observe a good coherence between T1 and T2.

Figures 10a–d give the classic features of SST in TIVs with cool SSTs in the southwest, where downwelling occurs (maximum -15 m day^{-1}), and warm SSTs in the upwelling region ($+5$ m day^{-1}), in agreement with PICOLO observations (see section 3b). It is reassuring that such features can be found using particle properties. This confirms the robustness of the method. In the depth-averaged view, maximum temperature changes occur in the southern quadrant of the vortices, with a strong cooling to the south and a weak warming to the north (Figs. 10e,f). The maximum cooling rate of 0.3°C day^{-1} is found at the transition between upwelling and downwelling (see Figs. 10c,d). At that location, the thermocline is shallow (Figs. 10g,h), the mixed layer is thin, strong vertical mixing occurs in the TIV, and there

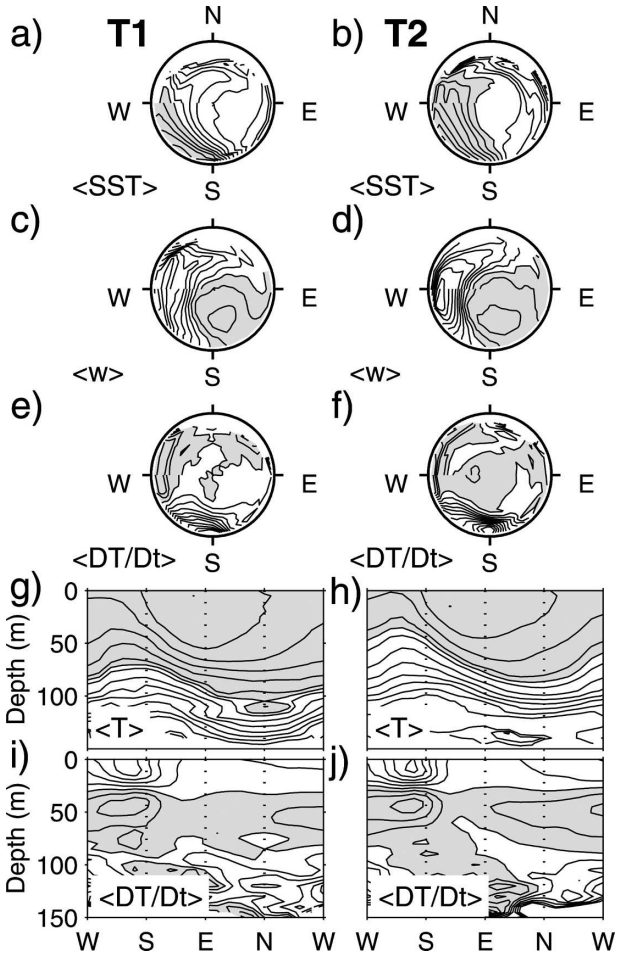

FIG. 10. (a), (c), (e), (g), (i) T1 and (b), (d), (f), (h), (j) T2 characteristics are shown. In (c), (d), (e), (f), (i) and (j), gray-shaded areas indicate positive values. All parameters are computed from the properties of those particles that remain in a vortex for at least 20 days, as a function of polar angle and depth in the vortex frame of reference. Fields are averaged over the (c)–(f) TIV depth and (g)–(j) vortex radius. (a), (b) Ensemble mean SST. Temperatures colder than 25°C are shaded in gray; there is a 0.25°C contour interval. (c), (d) Ensemble mean vertical velocities, with a 2 m day^{-1} contour interval. (e), (f) Ensemble mean daily variation of temperature, with a 0.03°C day^{-1} contour interval. Temperatures warmer than 24°C are shaded in gray. (g), (h) Ensemble mean temperature. (i), (j) Ensemble mean daily variation of temperature, with a 0.05°C day^{-1} contour interval.

is cooling in the mixed layer and warming in the layer below (Figs. 10i,j). These cooling patterns are consistent with those found in the Eulerian Pacific study of Menkes et al. (2006). Bearing in mind the 3D circulation from the above section, this is a place where most warm surface water coming from the north is cooled while cold upwelled water is warmed to a lesser extent. Cooling over the TIV depth is dominant (Figs. 10e,f), indicating that the vertical diffusion of cold upwelling water (or equally, entrainment) overcomes heating by surface heat fluxes (Jochum and Murtugudde 2006). However, rather than moving this newly cooled water to the north in the mixed layer, TIVs tend to advect cool water downward at the front where they circulate at depth with weak mixing (Figs. 10i,j). Overall, in the northern part of the TIV, a comparatively weaker diabatic warming is found, indicating that heat flux there indeed dominates vertical diffusion to warm the water (Jochum and Murtugudde 2006). Because the signal is weak, it is likely that sources of heat external to the TIV intervene to maintain the warmest temperatures found to the north. A close examination of the exchanges between TIVs and their surrounding waters is hence needed.

6. Mass exchanges

Our definition allowed us to follow TIVs through the tropical Atlantic over 50 days, that is, more than twice their typical rotation period. This longevity indicates that TIVs are dynamically coherent structures. However, this neither indicates to what extent the water within the structure is renewed, nor quantifies the amount of carried water and its origin. We use experiment E2 to investigate mass transfers between the TIVs and their surroundings in detail.

a. Exchanges quantification

For each E2 set, following each individual trajectory and determining every day whether a particle initially inside a vortex is leaving or remaining, we computed depletion curves as a percentage of the initial number of particles present in the vortex (Fig. 11). Over one rotation, TIVs are not closed structures but show large exchanges with surrounding waters, because about 50% of their mass is renewed. The 50% remaining continue to rotate in the TIV for 20 days or more as described in the previous section. On the left panel, one can see that at its initial stage, the vortex is forming and therefore loses mass less rapidly. Consequently, above 60% of the water initially captured will remain in it. After about 5 days, TIV dynamics seem to reach a balance for which rates of water mass exchanges do not vary significantly, as suggested by the time consistency between depletion curves. Furthermore, mean depletion curves are similar for T1 and T2 (Fig. 11, right panel).

Those results imply that although simulated TIVs remain coherent flow structures all along their path, they exchange considerably with their environment. At the end of its journey across the Atlantic, a vortex has renewed almost all of the water it initially contained, re-

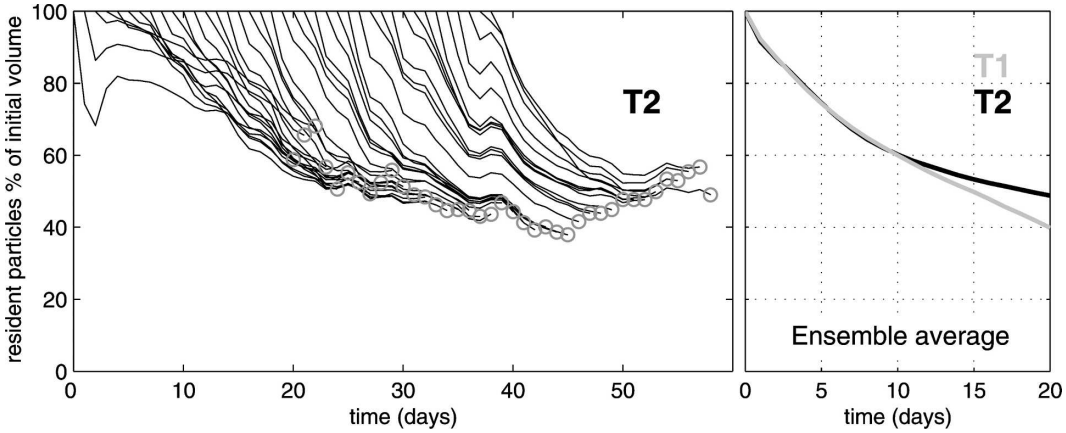

FIG. 11. (left) Particle depletion over 20 days (solid black) for every simulated day for vortex T2 in experiment E2. All depletion curves are normalized by their corresponding initial number of particles. Gray circles mark the remaining numbers of particles after one rotation cycle. (right) The ensemble average of the depletion curves for T1 (thick gray) and T2 (thick black).

distributing water on its way. How are these exchanges made, and what is their impact on the heat budget?

b. *Sources and sinks*

We can compute the particle positions as they enter or exit a vortex. Regridding these positions in the vortex frame of reference as a function of their polar angle from the east and depth, we obtain a detailed positioning for in- and outflowing for each day. On average (Fig. 12), three main water sources (black boxes) adjoin two main water sinks (white boxes). Water enters the TIV structures from the northwest (a vertically homogeneous source), the southeast (a surface-trapped source), and the southwest (a 50–100-m source). At the same time, water escapes from the vortex to the south (a sink) at middepth, around 50 m, and from the northeast (a vertically homogeneous sink). The depth-integrated value is plotted on top. For the sake of completeness, temperature is recomputed using inflow and outflow particle tracer characteristics (Fig. 12b). We aim to trace the fate and origins of these source/sink waters. To evaluate the inflow/outflow and residence time of entering particles, we computed percentages of the remaining particles from each source as a function of time over the vortex period (20 days). For the sinks, it is possible that particles leaving a vortex reenter it later. Thus, evaluation of particle numbers reentering the vortex during its rotation period is made. The ensemble means of these diagnostics for T1 and T2 are

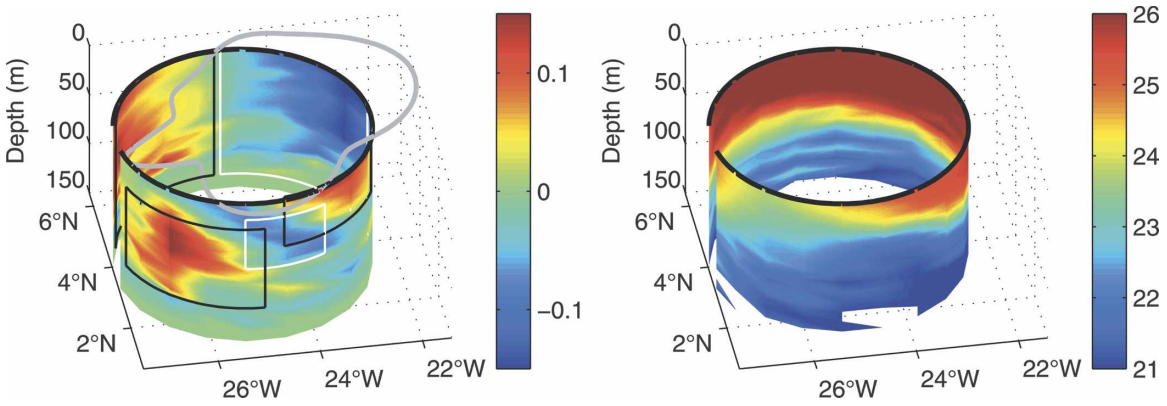

FIG. 12. (left) The ensemble mean particle inflow as a function of the total number of particles inside vortex T2. The gray line represents the depth integral of net inflow projected on the horizontal (at the surface) along the vortex contour (thick black line); inside values represent net inflow, outside values represent net outflow. Black rectangles indicate areas identified as sources for the vortex. White rectangles indicate areas identified as sinks. These areas are used in later diagnosis. (right) The ensemble mean temperature recomputed from inflowing/outflowing particle temperatures.

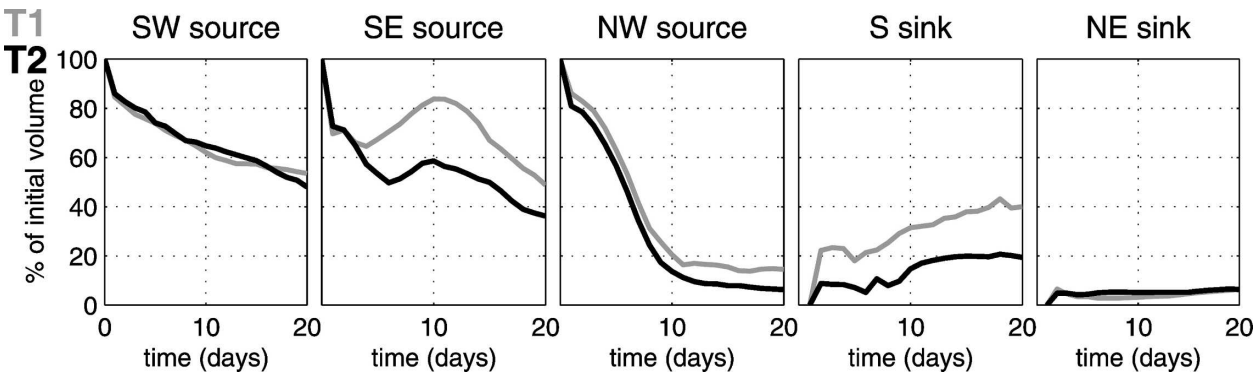

FIG. 13. All curves shown result from ensemble averaging from E2, for T1 (gray) and T2 (black). Sources are the number of particles originating in each of three sources defined in Fig. 12 and remaining in the vortex structure, which are presented with respect to time. Sinks are the number of particles coming back into the vortex structure and are presented as a function of time.

shown in Fig. 13. In the case of the sources, if all of the particles entering a vortex were remaining in it during the next revolution time scale, this percentage would steadily equal 100%.

This is not the case. All sources show a decrease in remaining particle numbers, indicating that some particles that enter indeed leave the vortex in the same revolution period. On average, after one rotation period, only 50% of the southwest source water effectively remains in a TIV. This water is being gradually expelled to the northeast and/or the south sinks (not shown). The path followed by particles from the southeast source is more intricate. About 5 days after their initial entry, 50% of particles already have left the structure through the south sink. Then, some come back from the southwest source as the vortex travels west. Eventually, about 50% still remain after one rotation period. Finally, the northwest source has almost entirely emptied in 10 days, mostly through the northeast sink.

Examination of the sinks shows that for the south sink, some particles that leave the structure reenter it progressively. After 10 days, 20% (for T2) to 40% (for T1) are reintroduced. This water was coming from the southeast source and later reentered through the southwest. Consistently, the percentage of water from the southeast source leaving and reentering is generally greater by 20% in T1 than in T2. Most of the water leaving to the northeast, however, does not come back into the vortex. Importantly enough, this means that most of the water acquired by the vortices is coming from the south of the vortex. We wish to locate the origin or fate of these waters passing through the vortices. To that end, particle position probability density functions 20 days before (after) entering (leaving) through each source (sink) are mapped for T2 (Fig. 14). Similar results are found for T1 (not shown).

The northwest source (Fig. 14a) consists of a complicated pattern of water coming mostly from the NECC, of water recirculated from the vortex 20 days before (see gray solid circle), and from the south. As particles enter the vortex, they bring warm water to the northern part of the vortex (see Fig. 12). This is probably the additional source of heat that is needed to maintain warm temperatures in the vortex's northern quadrant, as mentioned above. The particles eventually get expelled to the northeast (see before). From there, they either flow southward in the lee of the vortex, or they simply continue their route in the NECC (Fig. 14f). The southeast source water (Fig. 14b) consists mainly of SEC water and water contained in the vortex 20 days before. As particles enter the vortex, they bring warm water in the upper layers [see Fig. 12; this result is also found in heat advection examination by Menkes et al. (2006, see their Fig. 5c)]. The southwest source (Figs. 14d,e) displays the complexity mentioned above. SEC and recirculated water can enter through the southeast, exit in the south, and reenter in the southwest, or enter directly from the southwest. The latter contribution is made of thermocline equatorial water coming from the west via the upper part of the EUC. It enters the vortex at depth (the EUC depth) and brings cold temperatures (see Fig. 12). This is probably the main source maintaining the cold SST patterns of the vortex to the south. If TIVs are to bring Southern Hemisphere water to the north as mentioned by Foltz et al. (2004), it must come from the upper part of the EUC. Last, it is interesting to note that for the northeast and south sinks, some particles cross the equator, implying a Southern Hemisphere transfer of water masses via TIV dynamics. This pathway could be intuited from Fig. 1, where it can be seen that to the lee and the south of the TIV, the southward flow tends to cross the equator.

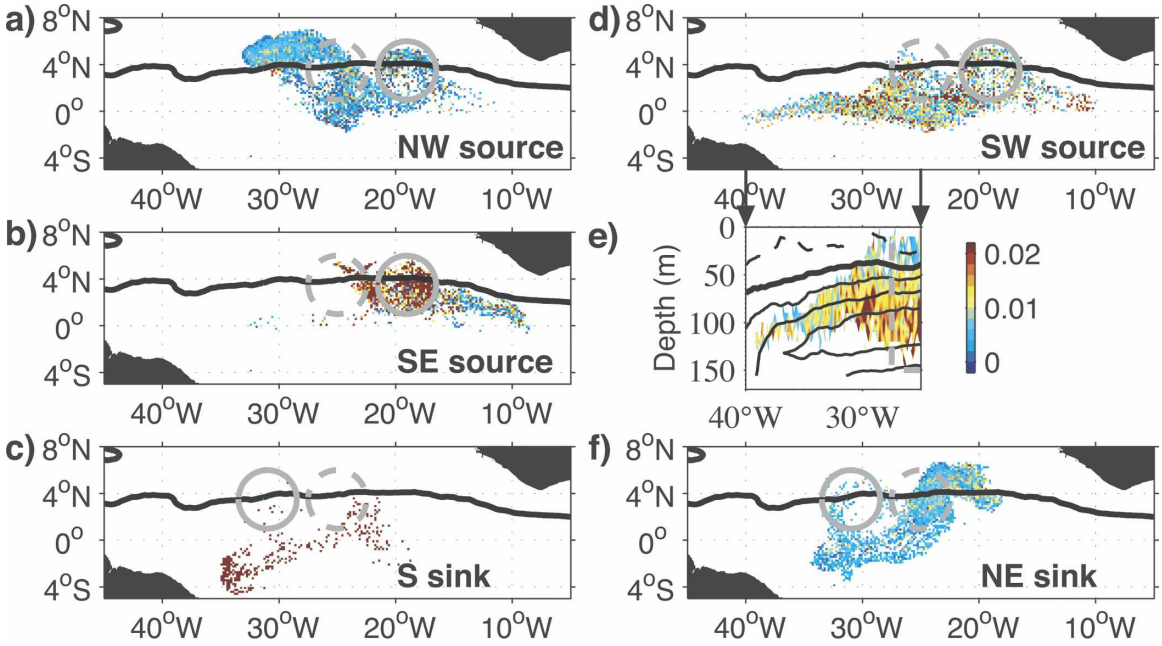

FIG. 14. Vortex T2 ensemble mean probability density function of water origin for each source (20 days before entering position) and water fate for each sink (20 days after exiting position). The gray solid circle represents T2 position when the probability density function is calculated. The gray dashed circle represents T2 hypothetical position 20 days before (for sinks) or after (for sources). Indicative mean positions of the vortex in the tropical Atlantic are chosen. (a) Northwest source, (b) southeast source, (c) south sink, (d) southwest source, and (f) northeast sink are shown; the probability density function is horizontal, integrated on the vertical. Null mean zonal current during the TIV activity period is drawn in solid black. (e) The southwest source; the probability density function is vertical, integrating on the horizontal. Mean zonal current west of 25°W at the equator during the TIV activity period is drawn; the contour interval is 0.25 cm s^{-1} with positive values in solid black, negative values in dashed black, and zero contour in thick solid black.

7. Summary and discussion

We have used a 1/6° model (CLIPPER) to simulate the dynamics of tropical instability wave vortices (TIVs) during 1997. The simulation is able to reproduce convincing 3D velocity and tracer fields during the summer time frame of the PICOLO cruise. To evaluate the effect of vortices on mass and heat redistribution, a Lagrangian point of view is taken. Particles seeding the vortex's active region are followed backward and forward. First, an experiment where floats are forced to remain at the surface is compared with a 3D experiment lasting 2 months. Profound differences are found using 2D experiments leading to particle concentration in convergence areas, thus undersampling a vast majority of the domain and in particular, the TIVs. To distinguish between vortices and their surroundings, we use a streamfunction-based criterion extended down to the upper thermocline (21°C) that is shown to define dynamically coherent 3D structures and allows diagnosis of daily inflows and outflows. Consistent with observations, TIVs present a 3D circulation that is not confined to the mixed layer but to the upper thermocline. These vortices have 20-day periods and 500-km diameters, but the particles that effectively rotate in them during a period experience only 2°–4° zonal and meridional excursions. Particles in the vortex typically have a spiraling movement; they experience upwelling in the southeast corner and downwelling in the southwest corner, leading to vertical excursions of 50 m. In 10 days, northern warm water has circulated to the south and is concentrated at the surface, while southern cold water sinks to the north. In 20 days, the mixture of horizontal spiraling and vertical movements redistribute particles in a complex and inhomogeneous manner. These vortices are not well represented by the solid body rotation model. The temperature of vortex-trapped particles changes by 1°–2°C in one rotation. This mainly occurs to the south of the vortex via vertical diffusion, where the thermocline is shallow and the vertical flow switches from upwelling to downwelling. The vertical diffusion cools the surface mixed layer water and heats the water below to a lesser extent. To the north (in the NECC), the effect is weak. In an Eulerian point of view, this means that heat is gained in the southern portion of TIVs (the SEC), while the north experiences almost no changes, a result that is fully consistent with those of Jochum and Murtugudde

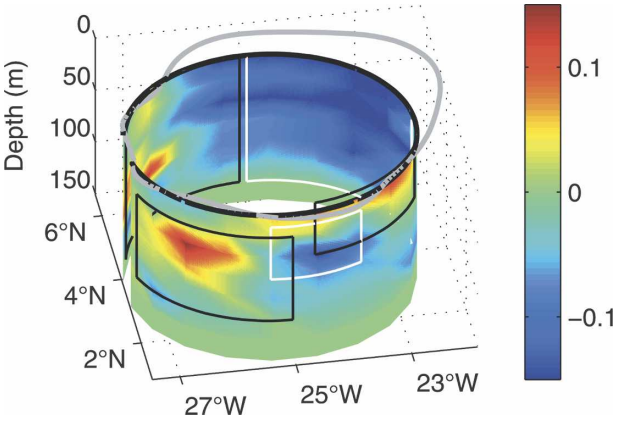

FIG. 15. Ensemble mean net (i.e., after 20 days) particle inflow as a function of the total number of particles originally inside vortex T2. The gray line represents the vertical integral projected at the surface. Black and white rectangles are the same as for Fig. 12. This figure represents the mean 3D structure of inflow responsible for the depletion of vortex water as shown in Fig. 11.

(2006) and Menkes et al. (2006). Next, we analyze the exchanges between TIVs and the surroundings. After 20 days, TIVs have lost 50% of their initial mass. There are three sources of water for TIVs. In the northwest, NECC water flows in at all depths, bringing warm water. In the southeast, water mostly recirculated in the vortex days before reentering at the surface, bringing warm water. In the southwest, upper EUC water and SEC water flow in mostly under the mixed layer. This is the main source of cold water to the TIV. This maintains the efficiency of vertical mixing that cools the recirculating water from the northern part of the TIV. Water is lost from the TIV via two routes—a weak southern sink and a northeastern sink, symmetric to the northwestern source. Both sinks tend to eject water to the south, down to the Southern Hemisphere. This corresponds to a southward flow that is systematically found in the lee of TIVs. It is worth examining the net inflows/outflows for TIVs over one period, defined as the number of inflowing (outflowing) particles still captured in (out of) the TIW after 20 days. Figure 15 describes the ensemble average of the net effect. This corresponds to the 3D structure associated with the depletion shown in Fig. 11 after 20 days. Overall, losses prevail, mostly through the northeast, which explains the water loss of 50% in 20 days. The main sources that maintain the vortex mass are located in the south (southwest and southeast), with the southwest source being dominant. By contrast, water entering in the north leaves the vortex more rapidly. Globally, depth-averaged values show that the southwest, southeast, and north sources account, respectively, for 60%, 25%, and 15% of the net inflow over a TIV period.

Discussion

Of the water initially contained, 50% still remains after one rotation period, and moves 5°–8° westward. Using a westward translation speed of 38 cm s^{-1}, a vortex in solid body rotation would have displaced its water 6° to the west in 20 days. TIVs are thus both transporting mass and exchanging with their surroundings.

In general, a vortex is seen as a body of water in rotation that is more or less isolated from its surroundings. On the contrary, a dispersive linear wave can have a similar current signature, but will not transport mass. Even in a nonlinear regime, Stokes drift cannot arguably give rise to the strong transports discussed here. TIVs thus appear to be on the fringe of the two cases, because they transport mass zonally over long distances, but still exchange a significant amount of properties with their environment. These dispersion and transport characteristics could well be due to a simple addition of linear or nonlinear wave (such as the observed unstable Rossby and Yanai waves; Lyman et al. 2007) effects, under Lagrangian chaos [see Bohr and Hansen (1996) for a simple example of the phenomenon].

The simplification of the problem to the study of enclosed vortices led us to construct somewhat arbitrary boundaries for TIVs. However, we did not find any definite criterion alleviating the ambiguity on TIV structures. For example, Foltz et al. (2004) also took other subjective criteria, finding similar characteristics for their vortices. We have checked the robustness of our method through a series of visual inspections of the particle movements using other streamfunction thresholds and vorticity-based criteria. Overall, the robustness of our results for two different vortices and the coherence of their 3D circulation with respect to observations also lead us to conclude that our results will not be strongly modified using other methods. In addition, our close examination of sources and sinks (section 6b) completes the analysis, and allows for more flexibility in our diagnostics.

One source of error that was not checked might come from the offline trajectory computations that rely on the hypothesis that the flow is constant over successive time periods equal to the nominal model output frequency. An initial evaluation using 5-day averages (instead of the daily averages used here) gave qualitatively similar results, but with significant quantitative differences for water mass trajectory and exchanges. Menkes et al. (2006) showed, using daily model output, that except for vertical diffusion processes, heat budget terms could be recovered almost exactly. For vertical diffusion, they estimated that the error attributable to

offline computation was 20%. Here, we are not subject to such errors because we estimated vertical diffusion processes directly by means of our methodology.

McCreary and Yu (1992) and Pezzi and Richards (2003) showed that TIW characteristics are sensitive to lateral mixing parameterizations. Although CLIPPER uses isopycnal diffusion for tracers, as recommended by Lengaigne et al. (2003) and Pezzi and Richards (2003), the robustness of our results may be questioned. Considering heat budgets at TIW scales, Menkes et al. (2006) and Peter et al. (2006) revisited this particular issue. Their conclusions did not reveal profound changes due to lateral parameterization. Because we are using the same base simulation as Peter et al. (2006), we would expect our results to remain equally robust.

Our results have shown that the EUC is a major water source for TIVs. Part of its water is then diverted to the north through these vortices. This export pathway has not yet been explored because typical EUC transport evaluations are usually based on time scales averaging TIV effects (Blanke and Raynaud 1997). That effect is expected to be stronger in the Pacific where TIWs are present almost year-round and cover a vast domain. Hence, evaluating such an effect is worth additional investigation.

We have seen that the balance between surface fluxes and vertical mixing in the TIVs is a major factor of temperature change (Jochum and Murtugudde 2006). The simulation considered here has constant surface heat fluxes over the TIV scales. Yet, observations and modeling results have demonstrated that heat fluxes are clearly structured at such scales (e.g., Liu et al. 2000; Small et al. 2003). Thus, additional study is required to investigate such effects.

Finally, observations have shown that the fronts between cold and warm SSTs in TIVs (where most mixing occurs) and the associated downwelling are much greater than those usually modeled. For instance, Johnson (1996) and Sawyer (1996) have mentioned that downwelling at the front could reach $O(500\ \text{m day}^{-1})$. To our knowledge, models so far are unable to produce such frontal velocities at TIV fronts. Thus, there still needs to be a detailed investigation of the frontal area in TIVs to understand the processes at play, and in particular the crucial role of mixing.

Acknowledgments. We thank IRD and LODYC for support and IDRIS for computer support. Author Pierre Dutrieux was also supported by NSF Grant OCE05-50857. Dr. E. Firing's help has been crucial throughout this work, from securing funding to providing insight. We thank Sean Kennan, Francois La-Mascagne, F. Ascani, and C. de Boyer Montegut for their comments and encouragement on an earlier version of the manuscript. Thanks are also addressed to two anonymous reviewers for their comments and suggestions.

REFERENCES

Arakawa, A., 1972: Design of the UCLA general circulation model. Numerical simulation of weather and climate. Department of Meteorology, University of California, Tech. Rep. 7, 116 pp.

Archer, D., and Coauthors, 1997: A meeting place of great ocean currents: Shipboard observations of a convergent front at 2°N in the Pacific. *Deep-Sea Res. II,* **44,** 1827–1849.

Baturin, N. G., and P. P. Niiler, 1997: Effects of instability waves in the mixed layer of the equatorial Pacific. *J. Geophys. Res.,* **102,** 27 771–27 794.

Blanke, B., and P. Delecluse, 1993: Variability of the tropical Atlantic Ocean simulated by a general circulation model with two different mixed-layer physics. *J. Phys. Oceanogr.,* **23,** 1363–1388.

——, and S. Raynaud, 1997: Kinematics of the Pacific Equatorial Undercurrent: An Eulerian and Lagrangian approach from GCM results. *J. Phys. Oceanogr.,* **27,** 1038–1053.

Bohr, T., and J. L. Hansen, 1996: Chaotic particle motion under linear surface waves. *Chaos,* **6,** 554–563.

Bracco, A., J. LaCasce, C. Pasquero, and A. Provenzale, 2000: The velocity distribution of barotropic turbulence. *Phys. Fluids,* **12,** 2478–2488.

Chavez, F. P., P. G. Strutton, G. E. Friederich, R. A. Feely, G. Feldman, D. G. Foley, and M. J. McPhaden, 1999: Biological and chemical response of the equatorial Pacific Ocean to the 1997–1998 El Niño. *Science,* **286,** 2126–2131.

Chelton, D. B., F. J. Wentz, C. L. Gentemann, R. A. de Szoeke, and M. G. Schlax, 2000: Satellite microwave SST observations of transequatorial tropical instability waves. *Geophys. Res. Lett.,* **27,** 1239–1242.

CLIPPER Project Team, 2000: 1/6° Atlantic circulation model forced by the ECMWF climatology: Preliminary results. Laboratoire de Physique des Océans Rep. 00-01, 130 pp. [Available online at http://www.ifremer.fr/lpo/clipper/result16/atl6/projet_clipper.htm.]

Cox, M. D., 1980: Generation and propagation of 30-day waves in a numerical model of the Pacific. *J. Phys. Oceanogr.,* **10,** 1168–1186.

Donohue, K., and M. Wimbush, 1998: Model results of flow instability in the tropical Pacific Ocean. *J. Geophys. Res.,* **103,** 21 401–21 412.

Flament, P., S. C. Kennan, R. A. Knox, P. Niiler, and R. L. Bernstein, 1996: The three-dimensional structure of an upper ocean vortex in the tropical Pacific Ocean. *Nature,* **383,** 610–613.

Foltz, G. R., J. A. Carton, and E. P. Chassignet, 2004: Tropical instability vortices in the Atlantic Ocean. *J. Geophys. Res.,* **109,** C03029, doi:10.1029/2003JC001942.

Gibson, J. K., P. Kallberg, S. Uppala, A. Nomura, A. Hernandez, and E. Serrano, 1997: ERA description. ECMWF Re-Analysis Project Report Series 1, 72 pp.

Gorgues, T., C. Menkes, O. Aumont, J. Vialard, Y. Dandonneau, and L. Bopp, 2005: Biogeochemical impact of tropical insta-

bility waves in the equatorial Pacific. *Geophys. Res. Lett.,* **32,** L24615, doi:10.1029/2005GL024110.

Haller, G., 2000: Finding finite-time invariant manifolds in two-dimensional velocity fields. *Chaos,* **10,** 99–108.

Hansen, D. V., and C. A. Paul, 1984: Genesis and effects of long waves in the equatorial Pacific. *J. Geophys. Res.,* **89,** 10 431–10 440.

Isern-Fontanet, J., J. Font, E. Garcia-Ladona, M. Emelianov, C. Millot, and I. Taupier-Letage, 2004: Spatial structure of anticyclonic eddies in the Algerian Basin (Mediterranean Sea) analyzed using the Okubo-Weiss parameter. *Deep-Sea Res. II,* **51,** 3009–3028.

Jochum, M., and R. Murtugudde, 2006: Temperature advection by tropical instability waves. *J. Phys. Oceanogr.,* **36,** 592–605.

Johnson, E. S., 1996: A convergent instability wave front in the central tropical Pacific. *Deep-Sea Res. II,* **43,** 753–778.

——, and J. A. Proehl, 2004: Tropical instability wave variability in the Pacific and its relation to large-scale currents. *J. Phys. Oceanogr.,* **34,** 2121–2147.

Kennan, S. C., and P. J. Flament, 2000: Observations of a tropical instability vortex. *J. Phys. Oceanogr.,* **30,** 2277–2301.

Legeckis, R., 1977: Long waves in the eastern equatorial Pacific Ocean: A view from a geostationary satellite. *Science,* **197,** 1179–1181.

Lengaigne, M., G. Madec, C. Menkes, and G. Alory, 2003: Impact of isopycnal mixing on the tropical ocean circulation. *J. Geophys. Res.,* **108,** 3345, doi:10.1029/2002JC001704.

Liu, W. T., X. Xie, P. S. Polito, S.-P. Xie, and H. Hashizume, 2000: Atmospheric manifestation of tropical instability wave observed by QuikSCAT and Tropical Rain Measuring Mission. *Geophys. Res. Lett.,* **27,** 2545–2548.

Luther, D. S., and E. S. Johnson, 1990: Eddy energetics in the upper equatorial Pacific during the Hawaii-to-Tahiti shuttle experiment. *J. Phys. Oceanogr.,* **20,** 913–944.

Lyman, J. M., D. B. Chelton, R. A. deSzoeke, and R. M. Samelson, 2005: Tropical instability waves as a resonance between equatorial Rossby waves. *J. Phys. Oceanogr.,* **35,** 232–254.

——, G. C. Johnson, and W. S. Kessler, 2007: Distinct 17- and 33-day tropical instability waves in subsurface observations. *J. Phys. Oceanogr.,* **37,** 855–872.

Madec, G., P. Delecluse, M. Imbard, and C. Lévy, 1998: POA 8.1 Ocean general circulation reference manual. Notes du pôle modélisation de L'Institut Pierre-Simon Laplace, 91 pp. [Available from LODYC, Université Pierre et Marie Curie, Place Jussieu, 75252 Paris Cedex 05, France.]

Masina, S., S. G. H. Philander, and A. B. G. Bush, 1999: An analysis of tropical instability waves in a numerical model of the Pacific Ocean. Part II: Generation and energetics of the waves. *J. Geophys. Res.,* **104,** 29 637–29 661.

McCreary, J. P., and Z. Yu, 1992: Equatorial dynamics in a 2.5-layer model. *Prog. Oceanogr.,* **29,** 61–132.

Menkes, C., and Coauthors, 2002: A whirling ecosystem in the equatorial Atlantic. *Geophys. Res. Lett.,* **29,** 1553, doi:10.1029/2001GL014576.

——, J. G. Vialard, S. C. Kennan, J.-P. Boulanger, and G. V. Madec, 2006: A modeling of the impact of tropical instability waves on the heat budget of the eastern equatorial Pacific. *J. Phys. Oceanogr.,* **36,** 847–865.

Niiler, P. P., R. E. Davis, and H. J. White, 1987: Water-following characteristics of a mixed layer drifter. *Deep-Sea Res.,* **34A,** 1867–1882.

Okubo, A., 1970: Horizontal dispersion of floatable particles in the vicinity of velocity singularities such as convergences. *Deep-Sea Res.,* **17,** 445–454.

Pasquero, C., A. Provenzale, and A. Babiano, 2001: Parameterization of dispersion in two-dimensional turbulence. *J. Fluid Mech.,* **439,** 279–303.

Peter, A.-C., M. Le Hénaff, Y. du Penhoat, C. E. Menkes, F. Marin, J. Vialard, G. Caniaux, and A. Lazar, 2006: A model study of the seasonal mixed-layer heat budget in the tropical Atlantic. *J. Geophys. Res.,* **111,** C06014, doi:10.1029/2005JC003157.

Pezzi, L. P., and K. J. Richards, 2003: Effects of lateral mixing on the mean state and eddy activity of an equatorial ocean. *J. Geophys. Res.,* **108,** 3371, doi:10.1029/2003JC001834.

Philander, S. G. H., 1976: Instabilities of zonal equatorial currents: I. *J. Geophys. Res.,* **81,** 3725–3735.

——, 1978: Instabilities of zonal equatorial currents: II. *J. Geophys. Res.,* **83,** 3679–3682.

Qiao, L., and R. H. Weisberg, 1998: Tropical instability wave energetics: Observations from the tropical instability wave experiment. *J. Phys. Oceanogr.,* **28,** 345–360.

Reynaud, T., P. Legrand, H. Mercier, and B. Barnier, 1998: A new analysis of hydrographic data in the Atlantic and its application to inverse modeling study. *International WOCE Newsletter,* No. 32, WOCE International Project Office, Southampton, United Kingdom, 29–31.

Richards, K. J., and N. R. Edwards, 2003: Lateral mixing in the equatorial Pacific: The importance of inertial instability. *Geophys. Res. Lett.,* **30,** 1888, doi:10.1029/2003GL017768.

Sawyer, M., 1996: Convergence and subduction at the North Equatorial Front. M.S. thesis, School of Ocean and Earth Science and Technology, University of Hawaii at Manoa, 92 pp.

Small, R. J., S.-P. Xie, and Y. Wang, 2003: Numerical simulation of atmospheric response to Pacific tropical instability waves. *J. Climate,* **16,** 3723–3741.

Strutton, P. G., J. P. Ryan, and F. P. Chavez, 2001: Enhanced chlorophyll associated with tropical instability waves in the equatorial Pacific. *Geophys. Res. Lett.,* **28,** 2005–2008.

Swenson, M. S., and D. V. Hansen, 1999: Tropical Pacific Ocean mixed layer heat budget: The Pacific cold tongue. *J. Phys. Oceanogr.,* **29,** 69–81.

Weidman, P. D., D. L. Mickler, B. Dayyani, and G. H. Born, 1999: Analysis of Legeckis eddies in the near-equatorial Pacific. *J. Geophys. Res.,* **104,** 7865–7888.

Weingartner, T. J., and R. H. Weisberg, 1991: On the annual cycle of equatorial upwelling in the central Atlantic Ocean. *J. Phys. Oceanogr.,* **21,** 68–82.

Weiss, J., 1981: The dynamics of enstrophy transfer in two-dimensional hydrodynamics. *Physica D,* **48,** 273–294.

Yoder, J. A., S. G. Ackleson, R. T. Barber, P. Flament, and W. Balch, 1994: A line in the sea. *Nature,* **371,** 689–692.

Yu, Z., J. P. McCreary, and J. A. Proehl, 1995: Meridional asymmetry and energetics of tropical instability waves. *J. Phys. Oceanogr.,* **25,** 2997–3007.